19th Australasian Fluid Mechanics Conference
Melbourne, Australia
8-11 December 2014

Wake Dynamics of Circular Finite Wall-mounted Cylinders in Different Boundary Layers

R. Porteous[1], D. J. Moreau[1], C. J. Doolan[1],and Z. Prime[1]

[1]Department of Mechanical Engineering
University of Adelaide, Adelaide, South Australia, 5005 AUSTRALIA

Abstract

A circular finite wall-mounted cylinder (FWMC) in cross-flow is common in many engineering applications including commercial buildings, heat exchangers, aircraft landing gear and automobile appendages. The wake shedding dynamics of such objects depends primarily on the aspect ratio (ratio of length to diameter, L/D) and the height of the incoming boundary layer (δ). Unlike the aspect ratio, the effect of the height of the boundary layer on wake flow is poorly understood. This paper presents unsteady wake measurements obtained behind a circular FWMC with $L/D = 18.2$ in two different boundary layers with $\delta/L = 0.1$ and 0.26, respectively. The results indicate that higher boundary layers alter the fluctuating characteristics of the wake at both the junction and free-end regions, even when the free-end lies significantly outside of the boundary layer itself.

Introduction

An FWMC is shown in Figure 1. The cylinder has one end immersed in the free stream (referred to as the 'free-end' or 'tip') and the other end fixed to a flat surface (referred to as the cylinder-wall 'junction') so that it is subject to a developing boundary layer of height δ. The cylinder is geometrically characterised by its span, L, and its diameter, D. The cylinder's aspect ratio is defined as L/D.

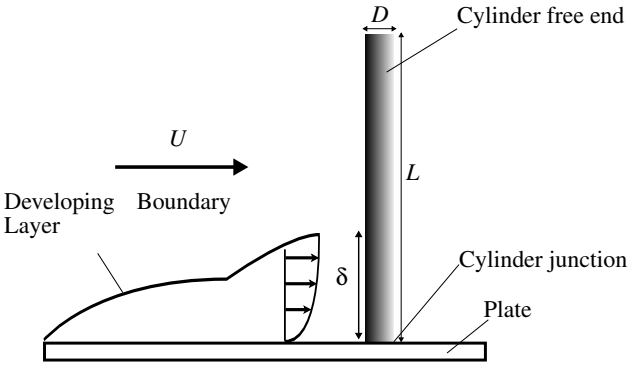

Figure 1: An FWMC mounted to a flat plate with a diameter, D and length, L subject to a flow with free stream velocity, U and an incoming boundary layer height of δ.

For a semi-infinite cylinder ($L \to \infty$), the wake is characterised by the periodic instability known as von Kármán vortex shedding. This flow phenomena occurs when the separated shear layer on one side of the cylinder rolls up in the wake and is subsequently shed as the process is continued on the opposite side [3]. The alternate shedding of vorticity occurs at a particular frequency, f_s, which is often represented in non-dimensional form by the Strouhal number based on cylinder diameter, $St = \frac{f_s D}{U}$ where U is the free stream velocity.

The presence of the free-end and junction region on an FWMC will substantially perturb the two-dimensional Kármán vortex wake structure, resulting in a change in shedding characteristics [6]. Lee [5] proposed that for $L/D > 12$, three 'cells' of vortex shedding will occur where the vortex shedding frequency varies in a stepwise manner along the span, where lower frequency cells are found at the free-end and junction respectively.

Kawamura et al. [4] found that the ratio of boundary layer height to span, δ/L, determines the aspect ratio where vortex shedding is suppressed. Sumner et al. [7] speculates that larger values of δ/L may influence the formation of vortex cells along the span of the cylinder but did not experimentally investigate this claim. Wang et al. [8] found that increasing δ/L for square FWMCs reduced downward directly flow over the free-end and weakens vortex shedding from the free-end. The dynamics of square FWMCs are, however, different from circular ones because the sharp leading edge promotes connectivity of vortex filaments across the whole cylinder [1], leading to an invarient vortex shedding frequency across the span. The impact that the boundary layer thickness has on the cellular nature of vortex shedding along the span of circular FWMCs has therefore not been researched. The aim of this paper is to investigate the dynamics of the vortex shedding in the wake of a circular FWMC when varying the boundary layer height. This is accomplished by comparing wake velocity data measured along the span of an FWMC in two different boundary layers.

Experimental setup

Wind Tunnel Facility

The experiment was conducted in the University of Adelaide's open-jet anechoic wind tunnel. The free jet exhausts into an anechoic room with internal dimensions of $1.4 \times 1.6 \times 1.8$ m. The jet nozzle is rectangular with a height of 75 mm and a width of 275 mm. The maximum flow velocity of the free-jet is approximately 30 m/s and the free-stream turbulence is 0.33 %.

Test Model

One circular FWMC was mounted perpendicular to a flat plate which was flush mounted to the jet nozzle, as shown in Figure 2. The flat plate measured 300×155 mm. The cylinder had a diameter, $D = 6.42$ mm, and a length L, of 116.53 mm. The aspect ratio, L/D, was therefore 18.20.

Measurement Equipment and Procedure

A TSI 1260A miniature hotwire probe was used to measure the incoming boundary layer and cylinder wake characteristics. The probe had a wire length of 1.27 mm and a wire diameter of 3.81 μm. The boundary layer profile was measured at the location of the cylinder with the cylinder removed. The cylinder wake was measured at a position $2D$ downstream (the x direction) and $1D$ laterally from the cylinder centreline (the y direction) at various position along the span of the cylinder (the z direction). The coordinate system and experimental setup is shown in Figure 2. The hotwire probe was connected to a Dantec automatic traverse with 6.25 μm accuracy allowing the hotwire to be traversed perpendicular to the plate. The hotwire was connected to a TSI IFA 300 Constant Temperature

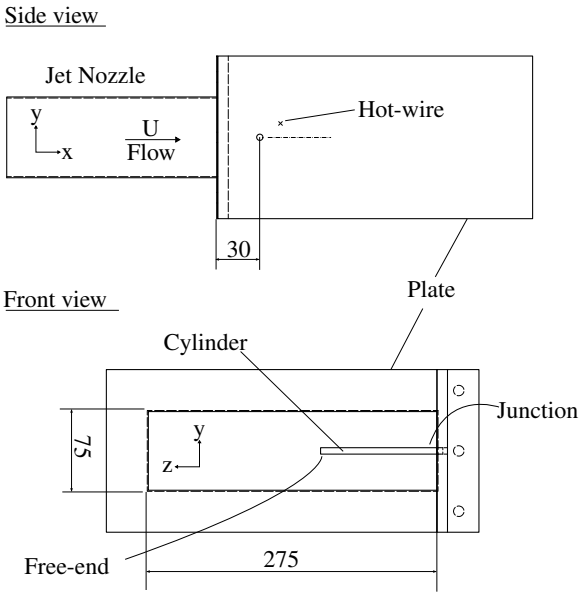

Figure 2: Schematic diagram of the experimental set up showing relative locations of hotwire probes. Coordinate system is as shown in the diagram.

Anemometry system. The CTA system was used in conjunction with Thermal Pro software to optimise the frequency response of the CTA circuit.

The experiment was run at a free-stream velocity of 29.5 m/s, producing a Reynolds number based on cylinder diameter of 1.2×10^4. Velocity fluctuations were sampled for 15 seconds at each measurement position at 2^{15} Hz using a DAQ with an automatic anti-aliasing filter. During the experiment, the hotwire was periodically calibrated after every boundary layer and cylinder measurement (approximately every 60 minutes) to minimise error due to hotwire drift. The temperature was monitored and observed to stay constant to within $\pm$ 0.5 degrees throughout the experiment and so was not corrected for. The measurement uncertainty associated with each hotwire measurement of mean velocity was estimated to be $\pm$ 0.1 m/s.

Boundary Layer

Two different boundary layers were used in this investigation; a low thickness turbulent boundary layer (LTB) that was allowed to develop naturally along wind tunnel contraction and a high thickness turbulent boundary layer (HTB) produced using an upstream tripping rod to thicken the boundary layer. The upstream tripping rod was 4 mm in diameter and located 180 mm ($28D$) upstream of the cylinder location.

Figure 3 compares the two boundary layer velocity profiles and turbulent intensity profiles at the position of the cylinder axis (with the cylinder removed). Table 1 compares the boundary layers' thickness, δ_{99}, displacement thickness, δ^*, momentum thickness, θ^*, shape factor, $H = \delta^*/\theta$ and $Re_\tau = \dfrac{\delta_{99} u_\tau}{\mu}$, where u_τ is the friction velocity of the two boundary layers. The results are normalised by the cylinder diameter, D where appropriate. The friction velocity was estimated by using curve fitting method of Coles [2].

Results

Figure 4 shows the spanwise distribution of mean velocity behind the cylinder as a function of normalised height, z/L, for

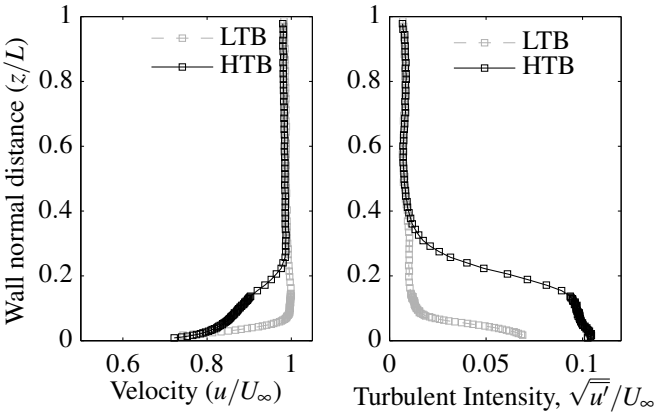

Figure 3: Mean and turbulent velocity profiles of the LTB and HTB.

	δ_{99}/D	δ^*/D	θ/D	H	Re_τ
LTB	1.4	0.47	0.29	1.57	714
HTB	4.4	0.56	0.42	1.31	2245

Table 1: Comparison of key boundary layer characteristics between the HTB and the LTB, normalised by cylinder diameter where appropriate.

both the LTB and HTB cases. Similarly, Figure 5 shows the spanwise distribution of turbulent intensity behind the cylinder.

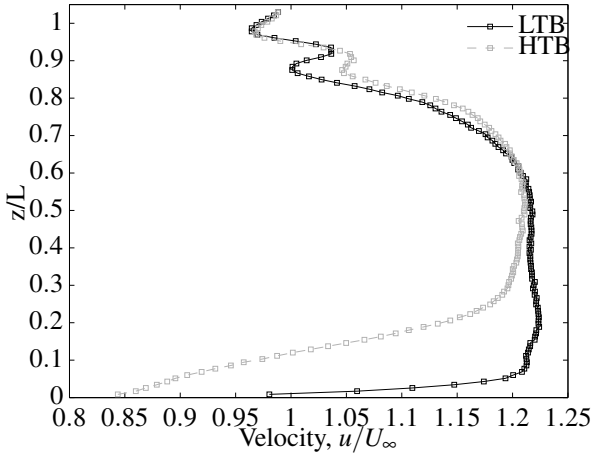

Figure 4: Comparison of spanwise variation in mean velocity for the HTB and LTB cases.

The mean velocity at the cylinder junction follows the profile of the boundary layer for each respective case. For example, in the HTB case, velocity shear occurs up to $z/L \approx 0.3$ due to the higher boundary layer. The velocity, however, is accelerated as it travels around the cylinder, and so the maximum velocity in Figure 4 is greater than that of the free-stream by approximately 6 m/s. Towards the free-end of the cylinder, the mean velocity decreases to that of the free-steam. This gradual decrease in velocity begins at $z/L \approx 0.6$ for both cases. The free-end is also characterised by a sudden increase in mean velocity at $z/L \approx 0.9$. This increase has a higher local maximum mean velocity in the HTB case compared with the LTB case.

At the cylinder junction ($0 < z/L < 0.3$), the turbulent intensity

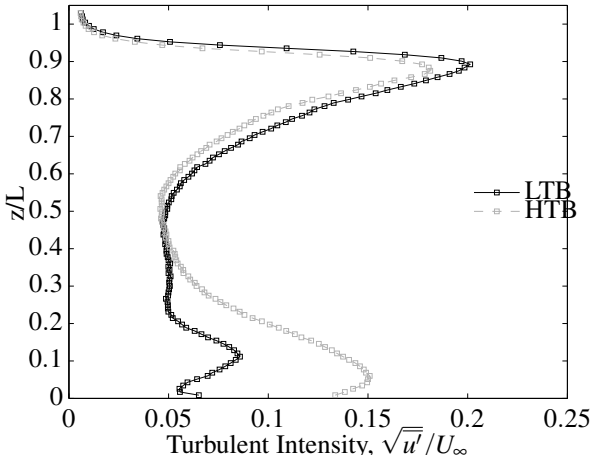

Figure 5: Comparison of spanwise variation in fluctuating velocity for the HTB and LTB cases.

levels for the HTB case are higher than the LTB case. Additionally, for the HTB case a local maximum in fluctuating level occurs closer to the junction, $z/L \approx 0.05$, than for the LTB case, for which the local maximum occurs at $z/L \approx 0.1$. For both boundary layers, the turbulent intensity tends to approach a steady level near the midspan of the cylinder, where the mean velocity is maximum. For the LTB case this occurs at $z/L \approx 0.2$, while for the HTB case, this occurs at $z/L \approx 0.4$. In the free-end region ($0.8 < z/L < 1$), the global maximum in turbulent intensity occurs at $z/L \approx 0.9$ for both boundary layers. However, the maximum levels for the HTB case in this region are less than that of the LTB case by $\Delta TI \approx 0.02$.

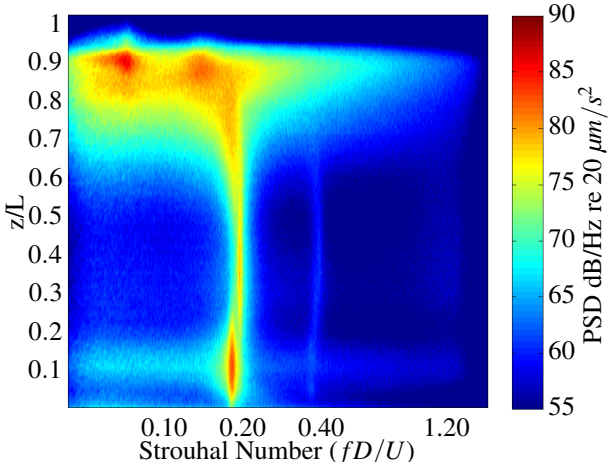

Figure 6: Spanwise variation of velocity power spectral density for the LTB case.

Figures 6 and 7 show the spanwise distribution of the velocity power spectral density (PSD) against Strouhal number, $St = fD/U$. In each figure, the PSD was estimated using Welch's averaged modified periodogram method with a Hanning window of length 16384 and 50% overlap. The 95% confidence interval on the narrowband PSD was therefore -0.96 dB / +0.8 dB.

From this spectral map, the fluctuating wake can be categorised into three-regions; (1) a midspan region where the fluctuating velocity is concentrated in a narrow band at $St = 0.2$ corresponding to vortex shedding, (2) a junction region, where the velocity fluctuation occurs at a slightly lower frequency, and (3)

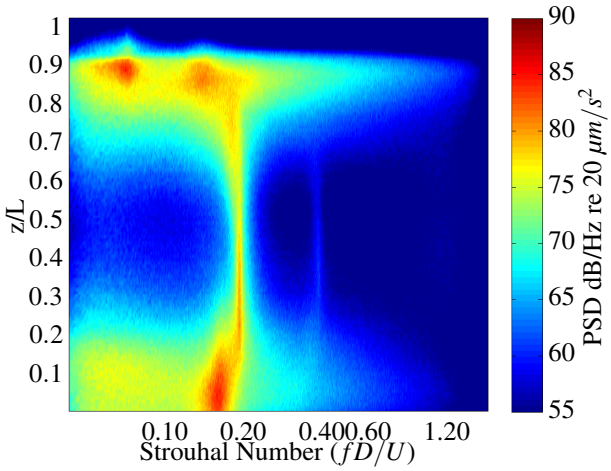

Figure 7: Spanwise variation of velocity power spectral density for the HTB case.

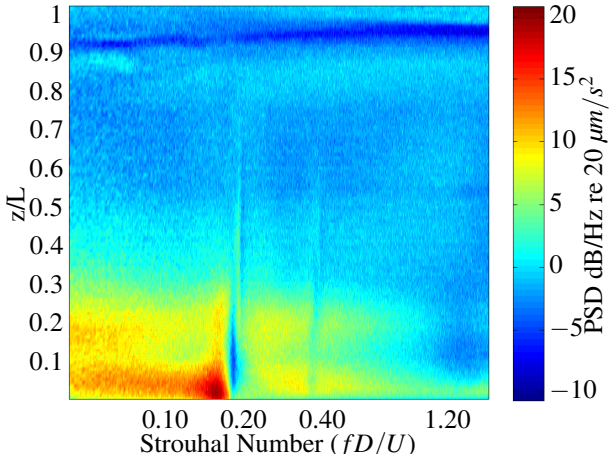

Figure 8: Difference in spanwise variation of velocity power spectral density between the HTB and LTB cases.

a free-end region where the fluctuating velocity is concentrated at $St = 0.07$.

Comparing Figures 6 and 7, the impact of the higher boundary layer is most prominent at the junction. The higher boundary layer raises the fluctuating energy level in the junction region for $St < 0.6$ and $0 < z/L < 0.25$. Additionally, the frequency of fluctuating velocity is reduced from $St = 0.18$ to $St = 0.16$.

Figure 8 shows the difference in fluctuating velocity between the LTB and HTB cases over the entire range of frequencies. This figure was produced by taking the difference between Figures 6 and 7. Apart from the large concentration of energy difference at $z/L < 0.3$, which has already been discussed, there is clear band of energy difference near the free-end at $z/L = 0.9$ over all frequencies. The disparity approximately 10 dB/Hz, which far exceeds the confidence intervals of the individual PSDs indicating that the difference in PSDs is significant. This implies that the fluctuating energy content at $z/L = 0.9$ is lower for the HTB case than for the LTB case. It is salient to note that the point $z/L = 0.9$ is $12D$ above the height of the HTB boundary layer.

Discussion

The results found in this study are in general agreement with the study of Wang et al. [8] for square FWMCs. In that study, it was also found that the relative height of boundary layer impacts the flow around the free-end, even when the free-end lies significantly away from the boundary layer. According to Wang et al. an increased boundary layer height increases upwash around the junction, which in-turn reduces downwash over the free-end. This promotes a higher probability of anti-symmetric shedding (vortices that shed with opposite phase either side of the cylinder) and a weakened the tip-vortex system at the free-end.

For the case of a circular cylinder, the vortex dynamics at the free-end are similarly impacted by the presence of the boundary layer. The significantly lower fluctuating velocity across all frequencies suggests that the vortex system at the free-end is weakened by the higher boundary layer. The mechanism for this weakened vortex system is unclear without directional information of the mean velocity in the cylinder wake. It may be plausible, however, that the downwash over the free-end is also reduced in the same manner as it is for square FWMCs. Since the magnitude of downwash flow has been directly related to the strength of the tip-vortex system [9], reduced downwash flow would signify a reduced strength tip-vortex.

Although the exact mechanism for the reduction of strength of the tip-vortex system is not exactly clear, the results do have implications for a wide range of engineering disciplines. For example, pollutants from chimney stacks can be directed towards the ground under the influence of downwash over the free-end of the chimney. The results of this study show that increasing the atmospheric boundary layer upstream of the chimney may be a simple way to reduce plume downwash. Another contemporary application of these results would be the reduction flow-induced noise generation from cylindrical appendages on transport vehicles, e.g the landing gear of an aeroplane. By tripping the boundary layer in front of the appendage, the tip-noise may be decreased.

Conclusions

The mean and turbulent wake characteristics of a circular FWMC of $L/D = 18.2$ in two different boundary layers were investigated using hotwire anemometry. The boundary layer heights were $1.4D$ and $4.4D$ and both had different turbulent characteristics. The results indicated that the incoming boundary layer can significantly impact the mean and turbulent wake characteristics of the FWMC. Specifically, it was shown that for a higher, more turbulent boundary layer, the junction region experienced higher overall turbulent intensity and lower frequency shedding. The midspan region of the FWMC generally remained unchanged between boundary layers. Interestingly, for the higher boundary layer, the free-end region experiences higher mean velocity and *less* overall turbulent intensity. This occurs despite the free-end region being far from edge of the boundary layer.

References

[1] Bourgeois, J., Sattari, P. and Martinuzzi, R., Alternating half-loop shedding in the turbulent wake of a finite surface-mounted square cylidner with a thin boundary layer, *Physics of Fluids*, **23**, 2011, 095101.

[2] Coles, D., The young person's guide to the data, in *Proceedings Computation of Turbulent Boundary Layer-1968 AFOSR-IPF-Stanford Conference*, Stanford University, 1968, volume 2.

[3] Gerrard, J. H., The mechanics of the formation region of vortices behind bluff bodies, *Journal of Fluid Mechanics*, **25**, 1966, 401 – 413.

[4] Kawamura, T., Hiwada, M., Hibino, T., Mabuchi, I. and Kumada, M., Flow around a finite circular cylinder on a flat plate (cylinder height greater than turbulent boundary layer thickness), *Bulletin of Japan Society of Mechanical Engineers*, **27**, 1984, 2142 – 2151.

[5] Lee, L., Wake structure behind a circular cylinder with a free end, *Proceedings of the heat transfer and fluids mechanics institute*, **35**, 1997, 241 – 251.

[6] Moreau, D. and Doolan, C. J., Flow-induced sound of wall-mounted finite length cylinders, *AIAA Journal*, **51**, 2013, 2493 – 2502.

[7] Sumner, D., Heseltine, J. and Dansereau, O., Wake structure of a finite circular cylinder of small aspect ratio, *Experiments in Fluids*, **37**, 2004, 720–730.

[8] Wang, H., Zhou, Y., Chan, C. K. and Lam, K. S., Effect of initial conditions on interaction between boundary layer and a wall-mounted finite-length-cylinder wake, *Physics of Fluids*, **18**, 2006, 065106.

[9] Wang, H. F., Cao, H. L. and Zhou, Y., Pod analysis of a finite-length cylidner near wake, *Experiments in Fluids*, **55**, 2014, 1790–1805.